Application of Physical Optics to the RCS Computation of Bodies Modeled with NURBS Surfaces

J. Pérez, *Student Member, IEEE*, and M. F. Cátedra, *Member, IEEE*

Abstract— **This paper presents a method for the computation of the monostatic radar cross section (RCS) of electrically large conducting objects modeled by nonuniform rational B-spline (NURBS) surfaces using physical optic (PO) technique. The NURBS surfaces are expanded in terms of rational Bezier patches by applying the Cox–De Boor transform algorithm. This transformation is justified because Bezier patches are numerically more stable than NURBS surfaces. The PO integral is evaluated over the parametric space of the Bezier surfaces using asymptotic integration. The scattering field contribution of each Bezier patch is expressed in terms of its geometric parameters. Excellent agreement with PO predictions is obtained. The method is quite efficient because it makes use of a small number of patches to model complex bodies, so it requires very little memory and computing time.**

I. Introduction

THE radar cross section (RCS) predictions of complex targets need a realistic modeling of the objects geometry. At this moment, the most popular technique for target description uses flat facets [1], [2]. One alternative is the nonuniform rational B-spline (NURBS) surfaces [3]–[6]. This technique is currently used in the aeronautic, automobile, ship, and other industries because it provides great advantages in complex objects' geometrical representation. The NURBS scheme is able to manipulate both free-form surfaces and primitive quadric surfaces (cylinders, spheres, cones, etc.) with a low number of patches, and therefore with a small amount of information. For instance, a primitive quadric like a cylinder can be modeled perfectly as only one NURBS surface; a complex body, such as a complete aircraft, can be described with nearly all its details, and a precision of 1 mm, by only a few hundred NURBS patches (see Fig. 1). Today, many of the available computer-aided geometric design (CAGD) tools provide descriptions of the designed objects in terms of NURBS curves and surfaces.

Apart from the above features, the use of NURBS patches provides important advantages in the description of bodies for RCS computation with regard to plane facets:

1) Artificial edges are not introduced.
2) Plane facets are a particular case of NURBS surfaces.
3) The number of patches is much lower.

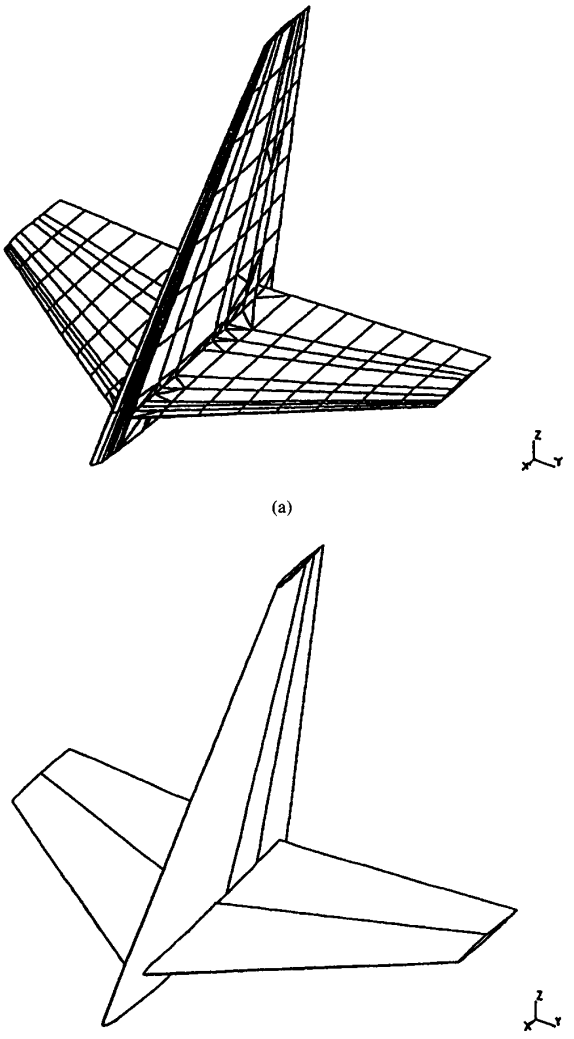

Fig. 1. Aircraft stabilizer models using (a) flat plates and (b) NURBS surfaces.

4) A better fit to the object geometry is provided.
5) Geometrical parameters of the body surface (normal vectors, curvatures, principal directions, etc.) are easy to obtain from the surfaces' description.

Manuscript received July 6, 1993; revised May 16, 1994. This work was supported by Dirección General de Telecomunicaciones (D.G.T.) and Construcciones Aeronaúticas Sociedad Anónima (C.A.S.A.) (No. Expte. 115.88.12.781.00, TIC:88-288E).

The authors are with the Departamento de Electrónica, Universidad de Cantabria, 39005 Santander, Spain.

IEEE Log Number 9404948.

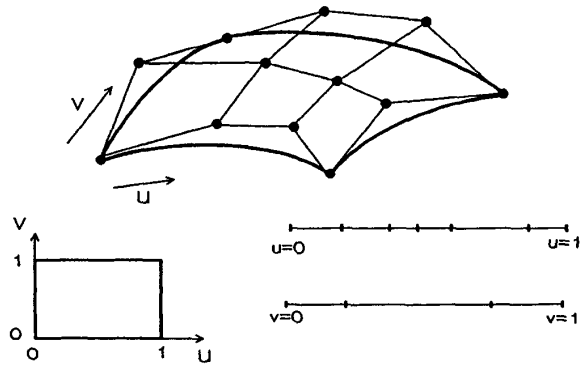

Fig. 2. NURBS surface geometric description.

The NURBS surfaces for the description of objects is starting to be used in RCS computation. One example is the GRECO code [7]. This code makes use of the NURBS technique for modeling the object geometry and, after this, a graphical-processing approach to an image of the target on the computer screen is used to obtain the unit normal at each point of the visible surfaces. With this information a high-frequency approximation to the RCS prediction is computed.

The method proposed in this paper works directly with the NURBS surfaces' parameters and provides expressions of the scattering field in terms of these parameters. The advantages with respect to the graphical-processing method is that it handles the real NURBS surfaces; on the other hand, the graphical-processing method works with a discretization of the surfaces (pixels).

A NURBS surface is a rational piecewise polynomial parametric surface. The coefficients of the polynomials depend on just a few control points (with associated weights) and two knot vectors (see Fig. 2). NURBS surfaces are quite useful for geometric designing for several reasons: They are invariant under affine transformations (rotation, scaling, translation, etc.) of the control points [3]. Another reason is the "local control" property [3]–[5]. This means that altering the position of a single data point causes only changes in a part of the surface. NURBS surfaces can be written like a combination of rational Bezier patches [3]–[5]. A rational Bezier patch is also a parametric surface defined in terms of a linear combination of Berstein polynomials [3], [5]. Bezier surfaces do not satisfy the local control property but are more suitable for the numerical computation of parameters associated with its geometry (curvatures, derivatives, integrations, etc.) thanks to the characteristics of the Berstein basis.

The transformation of NURBS into rational Bezier surfaces is straightforward by applying the Cox–De Boor algorithm [8]. Here, as in other applications of computational geometry, NURBS formats are used for the design and storage of the body's shape and the Bezier format for the surface interrogation of parameters such as point coordinates and parametric derivatives.

This paper presents a general method for the monostatic RCS computation of electrically large perfectly conducting objects modeled with NURBS surfaces. The PO approximation [9]–[12] is used, so it is implicity assumed that the radar frequency is high enough that the corresponding wavelength is small compared to the physical dimensions of the scattering body. Thus the scattering calculations are in the high-frequency region.

The PO integral is calculated as a sum of the individual contributions due to each Bezier surface. The patches are classified in four types according to its geometry: polygonal planes, planes with curved boundaries, singly curved surfaces, and double curved surfaces. When the patches are planes, the integral can be evaluated exactly. In the case of curved surfaces, the integrals are calculated over the parametric space of the corresponding Bezier surface by applying the stationary phase method [13]–[15]. It is straightforward to apply this technique to Bezier geometries. In a previous work [16], the authors presented a method for PO integral computation on curved surfaces. The stationary phase method was used, but only the main term of the integral asymptotic expansion was used. Therefore, the result was totally equal to the geometrical optics (GO) predictions [10]. In this paper, different order terms in the asymptotic expansion of the PO integral are taken into account, so the results are meaningfully improved. Finally, the individual contributions of all the Bezier patches are added in order to obtain the total scattering field.

In short, the method follows four steps:

1) Transformations of NURBS patches into rational Bezier surfaces,
2) Classification of the Bezier patches,
3) Computation of the backscattered field due to each Bezier surface by applying the stationary phase integration method, and
4) Sum of the backscattered fields of the individual patches; RCS computation.

This paper is organized as follows. Section II presents a brief introduction to the rational Bezier surfaces. Section III develops the method for the geometric classification of the Bezier surfaces. The technique used in order to calculate the backscattering field of each surface is introduced in Section IV. Sections V and VI present the expressions obtained by the application of the stationary phase method to the PO integral for the different kinds of curved patches. In Section VII, some RCS results obtained with this approach are presented and compared with PO predictions. Finally, the conclusions are outlined in Section VIII.

II. Rational Bezier Patches

The application of the Cox–De Boor algorithm to a NURBS surface provides a set of rational Bezier patches. The union of these patches makes up the primitive surface. The continuity between adjacent Bezier patches is determined by the knot vectors of the primitive NURBS surface [3].

The mathematical treatment of Bezier surfaces is simple. They are polynomial parametric surfaces normalized with a weight function. A Bezier patch is defined by two degrees (one for each parametric coordinate), a mesh of control points and a set of associated weights [3]–[5]. The coordinates of the surface points and their parametric derivatives functions are

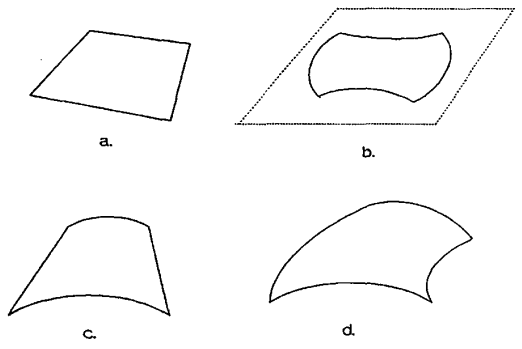

Fig. 3. (a) Polygonal plate, (b) plane patch with curved boundaries, (c) singly curved surface, and (d) double curved surface.

given in terms of linear combinations of Berstein polynomials that can be easily computed and are numerically stable [3]. The surface points of a rational Bezier surface are given by

$$\vec{r}(u,v) = \frac{\sum_{i=0}^{m}\sum_{j=0}^{n} w_{ij}\vec{b}_{ij}B_i^m(u)B_j^n(v)}{\sum_{i=0}^{m}\sum_{j=0}^{n} w_{ij}B_i^m(u)B_j^n(v)} \tag{1}$$

where $\vec{b}_{ij}$ are the control points, w_{ij} are the control points weights, $\mathbf{m}$ and $\mathbf{n}$ are the surface degrees, and $B_i^m(u)$ and $B_j^n(v)$ are the Berstein polynomials:

$$B_k^s(t) = \frac{s!}{k!(s-k)!}t^k(1-t)^{s-k}. \tag{2}$$

The number of Bezier patches obtained from a NURBS depends on its knot vectors [3], [5], [8]. Important features of the rational Bezier surfaces are as follows:

1) *Convex hull* property [3]–[6]. The surface points lie completely within the convex hull of the mesh of control points.
2) The boundary curves are rational Bezier curves [3]–[4]. Their control points are given by the boundary control points of the net. In particular, the four corners of the control net lie on the patch.
3) The parametric coordinates take values between 0 and 1. Therefore, the parametric space of the Bezier patches is a square with a side length of one.
4) The parametric derivatives can be calculated easily [3]–[4], using the Berstein polynomials properties.

III. Classifications of Rational Bezier Surfaces

The method used to compute the PO integral on a Bezier patch depends on the geometry of the Bezier surface. The patches are classified into four types (see Fig. 3).

Polygonal plane patches: Taking account the convex hull property, a Bezier patch is plane if all its control points are in the same plane. According to property 2, to be a polygonal patch the control points that define each boundary curve of the surface must be collinears. In the event that both degrees of the patch are equal to one, the previous condition is satisfied automatically because the mesh of control points is reduced to a polygonal facet with four vertices. In this case, if two control points coincide the patch will be a triangular facet.

Plane patches with curved boundaries: All the controls points are in the same plane, but the control points of at least one boundary of the net are not collinear. This implies that at least one of the surface degrees must be higher than one. A typical example is a disk.

Singly curved patches (ruled surfaces): These are generated by a family of straight lines [3]. In a optimized design these straight lines are isoparametrics. Typical examples are the cylindrical and conical surfaces.

In a optimized design, the singly curved Bezier patches verify one of the following two sets of conditions:

$$\begin{aligned} &n = 1 \\ &w_{i1} = w_{i0}, \quad i = 1,2,\cdots,m \end{aligned} \tag{3}$$

or

$$\begin{aligned} &m = 1 \\ &w_{1j} = w_{0j}, \quad j = 1,2,\cdots,n. \end{aligned} \tag{4}$$

In the first case, the surface is linear with the coordinate v and (1) can be written in the following form:

$$\vec{r}(u,v) = \vec{r}_0(u) + v\vec{r}_1(u) \tag{5}$$

where

$$\vec{r}_0(u) = \frac{\sum_{i=0}^{m} w_{i0}\vec{b}_{i0}B_i^m(u)}{\sum_{i=0}^{m} w_{i0}B_i^m(u)} \tag{6}$$

$$\vec{r}_1(u) = \frac{\sum_{i=0}^{m}(w_{i1}\vec{b}_{i1} - w_{i0}\vec{b}_{i0})B_i^m(u)}{\sum_{i=0}^{m} w_{i0}B_i^m(u)}. \tag{7}$$

Consequently, the second-order derivative with respect to v is zero in any point.

If the conditions of (4) are satisfied, the surface is linear with the coordinate u and the expression (1) can be written as

$$\vec{r}(u,v) = \vec{r}_0(v) + u\vec{r}_1(v) \tag{8}$$

where

$$\vec{r}_0(v) = \frac{\sum_{j=0}^{n} w_{0j}\vec{b}_{0j}B_j^n(v)}{\sum_{j=0}^{n} w_{0j}B_j^n(v)} \tag{9}$$

$$\vec{r}_1(v) = \frac{\sum_{j=0}^{n}(w_{1j}\vec{b}_{1j} - w_{0j}\vec{b}_{0j})B_j^n(v)}{\sum_{j=0}^{n} w_{0j}B_j^n(v)}. \tag{10}$$

In this case, the second-order derivative with respect to u is zero in any point.

Doubly curved patches (without restrictions): In general, the second parametric derivatives and the principal curvatures are distinctly zero.

IV. Bakscattering Field of a Rational Bezier Surface

Given an incident monochromatic plane wave, under the far field approximation, the backscattering field of an arbitrary conducting body predicted by PO [9]–[11] is given by

$$\vec{E}_s(\vec{r}) = -j\lambda^{-1}\vec{E}_0\frac{e^{-jKr}}{r}(\hat{K}\cdot\vec{I}) \tag{11}$$

$$\vec{I} = \int_s \hat{n}_s(\vec{r}')e^{2j\vec{K}\cdot\vec{r}'}ds' \tag{12}$$

where $\mathbf{S}$ is the body surface, λ is the wavelength, $\vec{E}_0$ is the incident electric field, $\vec{K}$ is the wave vector, $\hat{K}$ is the normalized wave vector, $\vec{r}'$ is the surface point corresponding to ds', and $\hat{n}_s$ is the unit normal vector at this point. Notice that the incident field and the predicted PO scattering field have the same polarization, and also that the monostatic RCS prediction will be independent of the incident wave polarization.

If the Bezier surface is plane, $\hat{n}_s(\vec{r}')$ is constant and (12) can be calculated using Gordon's method [17]. However, if $\mathbf{S}$ is an arbitrary curved Bezier surface, is not possible to calculate $\vec{I}$ analytically, and therefore the stationary phase method is used.

The integral can be expressed on the parametric coordinates of the Bezier patch writing the normal vector function and the surface element in terms of the parametric derivatives of $\vec{r}(u,v)(\vec{r}_u$ and $\vec{r}_v)$:

$$\hat{n} = \frac{\vec{r}_u\times\vec{r}_v}{|\vec{r}_u\times\vec{r}_v|} \tag{13}$$

$$ds = |\vec{r}_u\times\vec{r}_v|du\,dv \tag{14}$$

so,

$$\vec{I} = \int_{u=0}^{u=1}\int_{v=0}^{v=1}\vec{r}_u(u,v)\times\vec{r}_v(u,v)e^{2j\vec{K}\cdot\vec{r}(u,v)}du\,dv. \tag{15}$$

The integration is made in the parametric domain. It is a rectangle of corners (0, 0), (0, 1), (1, 0), (1, 1). In this domain the application of the stationary phase method is very easy. In the following sections the results of the asymptotic integration of (15) for the two kinds of curved Bezier surfaces are presented. All the asymptotic contributions are written in terms of $\vec{r}(u,v)$ and its parametric derivatives.

V. Doubly Curved Bezier Surfaces

The stationary phase method in double integrals [13], [15] shows that contributions come only from regions in the vicinity of certain critical points of the integral domain, and that different types of critical points give rise to different powers of $\mathbf{K}$ in the leading terms of their respective contributions. There are three types of critical points, as explained below.

A. Stationary Phase Points (Critical Points of the First Kind)

These are points within the domain of integrations on which (see Fig. 4)

$$\vec{K}\cdot\vec{r}_u(u_0,v_0) = 0,$$
$$\vec{K}\cdot\vec{r}_v(u_0,v_0) = 0. \tag{16}$$

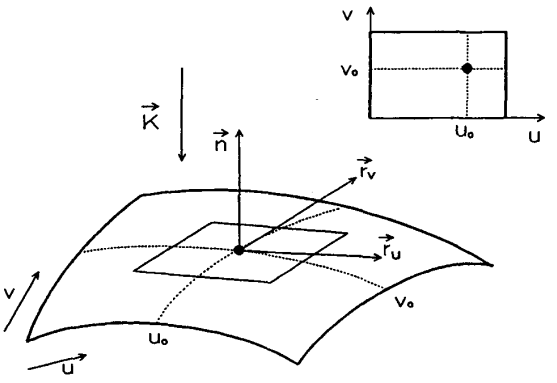

Fig. 4. Stationary phase point.

They are the so-called specular points. The contribution to $\vec{\mathbf{I}}$ is proportional to K^{-1} and is given by

$$\vec{\mathbf{I}} \simeq \sigma\pi e^{2j\vec{K}\cdot\vec{r}}\frac{(\vec{r}_u\times\vec{r}_v)}{|(\vec{K}\cdot\vec{r}_{uv})^2-(\vec{K}\cdot\vec{r}_{uu})(\vec{K}\cdot\vec{r}_{vv})|^{1/2}} \tag{17}$$

where σ is equal to $\mathbf{j}, -\mathbf{j}$, or $\mathbf{1}$, depending on whether (u_0, v_0) is a local minimum, local maximum, or saddlepoint, respectively, of the function $\vec{K}\cdot\vec{r}(u,v)$.

There may be more than one stationary point within the surface domain, and provided these points are well separated [14], the asymptotic evaluation of the integral is given by the sum of the individual contributions as in (17). If the points are close, the previous expression is not valid; it will be necessary to consider the coupling effect between the points. This cannot happen if the surfaces are smooth, and therefore it is not treated here.

These are the first-order contributions of the asymptotic integration of double curved surfaces, and they are exactly equal to the GO predictions [10].

B. Boundary Critical Points (Second Kind Points)

These are the points of the curve bounding the domain of integration on which one of the following expressions is verified (see Fig. 5):

$$\vec{K}\cdot\vec{r}_v(u=0,v_0) = 0; \quad \vec{K}\cdot\vec{r}_v(u=1,v_0) = 0,$$
$$\vec{K}\cdot\vec{r}_u(u_0.v=0) = 0; \quad \vec{K}\cdot\vec{r}_u(u_0,v=1) = 0. \tag{18}$$

Their contributions are proportional to $K^{-3/2}$ and are given by

$$\vec{I} \simeq j(-1)^\alpha e^{2j\vec{K}\cdot\vec{r}}\frac{\vec{r}_u\times\vec{r}_v}{2\vec{K}\cdot\vec{r}_\alpha}\left[\frac{j\pi}{(\vec{K}\cdot\vec{r}_{\beta\beta})}\right]^{1/2} \tag{19}$$

where α is u and β is v in the first and second cases; and α is v and β is u in the third and fourth cases.

As in the case of stationary points, the problem of close boundary points is not taken into account because the surface is considered smooth enough.

When a second kind point approaches a stationary phase point it is necessary to consider the coupling effect between

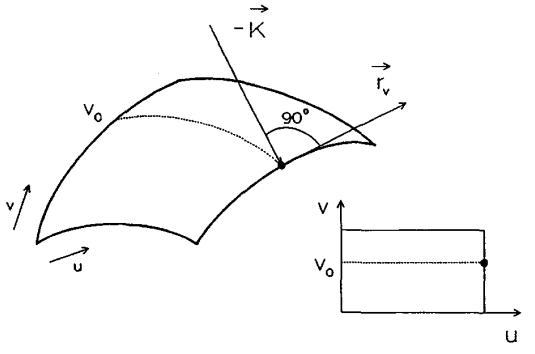

Fig. 5. Boundary critical point.

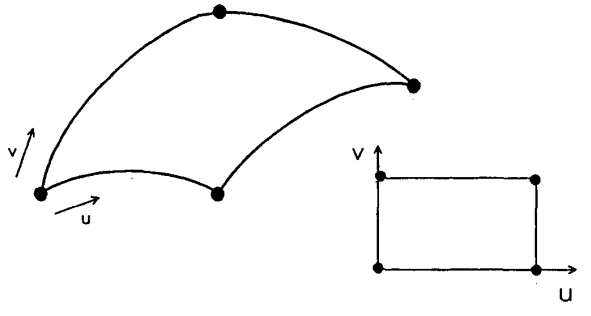

Fig. 6. Vertex points.

them. In this case, the term $[2\vec{K}\cdot\vec{r}_\alpha]^{-1}$ of (19) must be substituted by

$$-sj\left[\frac{1}{|\vec{K}\cdot\vec{r}_{\alpha\alpha}|}\right]^{1/2}\ \text{sign}\ (\vec{K}\cdot\vec{r}_\alpha)e^{-jsv_\alpha^2}F_s(v_\alpha) \tag{20}$$

where

$$s = \ \text{sign}\ (\vec{K}\cdot\vec{r}_{\alpha\alpha}) \tag{21}$$

$$v_\alpha = \frac{|\vec{K}\cdot\vec{r}_\alpha|}{(\vec{K}\cdot\vec{r}_{\alpha\alpha})^{1/2}} \tag{22}$$

and function F is the Fresnel integral.

If there is continuity in the first and second parametric derivatives in the connection between adjacent patches, these contributions vanish when the scattering field of these patches is added.

C. Vertex Points (Critical Points of the Third Kind)

In general, these are defined as the corner points of the curve bounding the domain of integration, that is, points at which the slope of the curve can be discontinuous [13], [15]. In the case of the Bezier patch domain the vertex points are the four corners: (0, 0), (0, 1), (1, 0), (1, 1) (see Fig. 6). Their contributions are proportional to K^{-2} and are given by

$$\vec{I}\simeq(-1)^{u+v}e^{2j\vec{K}\cdot\vec{r}}\frac{(\vec{r}_u\times\vec{r}_v)}{-4(\vec{K}\cdot\vec{r}_u)(\vec{K}\cdot\vec{r}_v)}. \tag{23}$$

When a vertex point is close to a stationary phase point or a critical boundary point, it is necessary to consider the coupling effect between them. In this event the previous expressions for stationary and boundary points are valid, but (23) must be modified. Then, the term $[(\vec{K}\cdot\vec{r}_u)(\vec{K}\cdot\vec{r}_v)]^{-1}$ must be replaced by

$$4\ \text{sign}\ (\vec{K}\cdot\vec{r}_u)\ \text{sign}\ (\vec{K}\cdot\vec{r}_v)\left[|\vec{K}\cdot\vec{r}_{uu}||\vec{K}\cdot\vec{r}_{vv}|\right]^{-1/2}T_uT_v \tag{24}$$

where

$$T_\alpha = jse^{-jsv_\alpha^2}F_s(v_\alpha) \tag{25}$$

$$s = \ \text{sign}\ (\vec{K}\cdot\vec{r}_{\alpha\alpha}) \tag{26}$$

As in the case of the boundary critical points, if there is continuity in the first parametric derivatives in the connection between adjacent patches, this contribution vanishes when the scattering field of these patches is added.

VI. Singly Curved Bezier Surfaces

If a Bezier patch is single curved, the phase term of integral (15) is linear and the second derivative of $\vec{r}(u,v)$ is equal to zero for one parametric coordinate (see (5) and (8)). In this case, the integration along the linear coordinate can be calculated analytically and the stationary phase method for single integrals is applied to evaluate the integral along the other coordinate.

For example, if the surface verifies (3), the integral along the coordinate u is calculated first using asymptotic integration and then the result obtained is integrated along the coordinate v analytically.

The PO integral can be written in this form:

$$\vec{I}=\int_{v=0}^{v=1}\vec{I}_u(v)dv \tag{27}$$

where the integral over the u coordinate,

$$\vec{I}_u(v)=\int_{u=0}^{u=1}\vec{r}_u(u,v)\times\vec{r}_v(u,v)e^{2j\vec{K}\cdot\vec{r}(u,v)}du \tag{28}$$

is approximated by the contributions to two types of critical values of the u coordinate, i.e., stationary phase and boundary values. These fixed values define two types of isoparametric curves on the surface. Because of the linearity of $\vec{r}(u,v)$ with the coordinate v, the isoparametric curves of u constant are segments on the surface. Then, the asymptotic contributions to PO integral in single curved patches are due to two types of critical segments on the patches: stationary phase segments and boundary segments.

A. Stationary Phase Segments

These are defined by the stationary phase points of the integral (28). The points of the segments verify $\vec{r}_u(u_s,v)=0$ (see Fig. 7), and their contributions are given by

$$\vec{I}_u(v)\simeq e^{2j\vec{K}\cdot\vec{r}}[\vec{r}_u\times\vec{r}_v]\left[\frac{\pi j}{\vec{K}\cdot\vec{r}_{uu}}\right]^{1/2}. \tag{29}$$

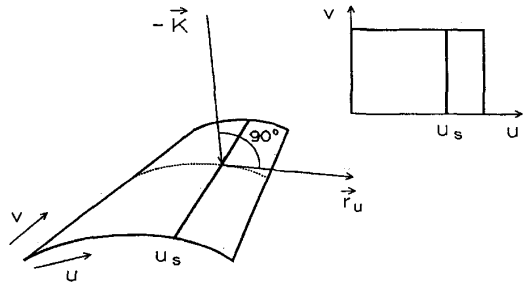

Fig. 7. Stationary phase segment.

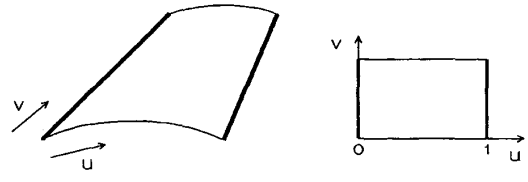

Fig. 8. Boundary segments.

B. Boundary Segments

These are defined by the boundary domain segments, with $u_0 = 0$ or $u_0 = 1$ (see Fig. 8). Both contributions are given by the following expression:

$$\vec{I}_u(v) \simeq j(-1)^{u_0} e^{2j\vec{K}\cdot\vec{r}} \frac{\vec{r}_u \times \vec{r}_v}{2\vec{K}\cdot\vec{r}_u}. \tag{30}$$

When a stationary phase segment is close to a boundary segment, (30) is not valid. It is necessary to consider the coupling effect between the segments [14], so in this case the boundary segments' contributions are given by

$$\vec{I}_u(v) \simeq s(-1)^{u_0} e^{2j\vec{K}\cdot\vec{r}} \cdot \frac{\vec{r}_u \times \vec{r}_v}{\sqrt{|\vec{K}\cdot\vec{r}_{uu}|}} \text{ sign } (\vec{K}\cdot\vec{r}_u) e^{-jsv_u^2} F_s(v_u) \tag{31}$$

where

$$s = \text{ sign } (\vec{K}\cdot\vec{r}_{uu}). \tag{32}$$

If the boundary segment is isolated from the stationary phase segments, (31) tends to (30).

All the segments contributions have the form

$$\vec{I}_u(v) \simeq \vec{G}(u_0, v) e^{jf(u_0,v)}. \tag{33}$$

The phase term of (33) is linear with the coordinate v (see (3)), so in order to evaluate (27) the amplitude term $\vec{G}(v)$ is developed in Taylor's series around the value $v = 0.5$. Therefore, (27) is transformed in a sum of integrals that can be calculated analytically. The result is

$$\vec{I} = \int_{v=0}^{v=1} \vec{I}_u(v) dv \simeq e^{jf_0} \sum_{n=0}^{N} \sum_{k=n}^{N} \frac{\vec{G}^{(k)}(-v_0)^{k-n} A_n}{(k-n)!n!} \tag{34}$$

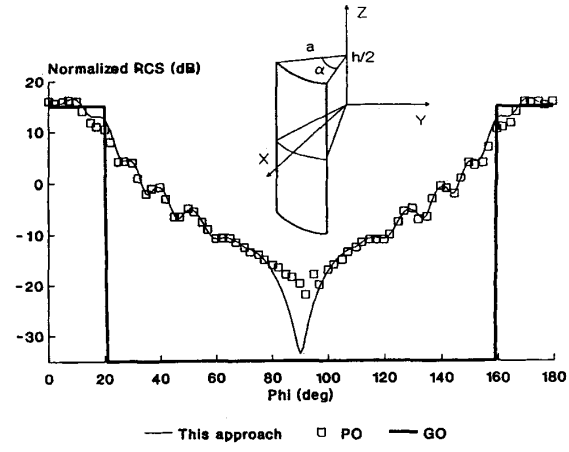

Fig. 9. RCS of a cylindrically curved plate along the $\theta = 90°$ cut.

where $\vec{G}^{(k)}$ is the kth term of the amplitude Taylor's series, N is the number of terms considered, and

$$A_n = \int_{v=0}^{v=1} v^n e^{jvf_v} dv = \frac{n!}{jf_v} \left\{ \left(\sum_{i=0}^{n} \frac{e^{jf_v}}{(-jf_v)^i (n-i)!} \right) - \frac{1}{(-jf_v)^n} \right\} \tag{35}$$

$$f_0 = 2\vec{K}\cdot\vec{r}(u_0, v_0) \tag{36}$$

$$f_v = 2\vec{K}\cdot\vec{r}_v(u_0, v_0.) \tag{37}$$

Analogous expressions are obtained when the patch is linear with the parametric coordinate u.

VII. Results

Numerical results of RCS for different geometries are presented below.

A. Cylindrically Curved Plate

Results with this geometry are presented in Fig. 9, where a sketch of the plate is shown. The height of the plate in the Z direction is $h = 12.8$ cm, the cylinder radius is $a = 16.3$ cm, the angle $\alpha = 40°$, and the frequency of the incident field 9.375 GHz. The target is modeled with one singly curved Bezier surface of degrees 1×2. Results from our approach are compared with values obtained from [18], which uses a numerical implementation of PO. The values are normalized with respect to h^2.

B. Spherically Curved Plate

This object is modeled with only one doubly curved Bezier surface of degrees equal to 2. A sketch of the plate is shown in Fig. 10. The plate extends over a beam of 90° for the θ and ϕ angles. The sphere radius is $a = 1$ m. Fig. 10 shows results for different values of frequency. The spherical coordinates of the incident wave directions are $\phi = 45°$ and $\theta = 90°$. Fig. 11 presents results for different incident wave directions in a $\phi = 45°$ cut and a frequency of 3 GHz. In both cases the results

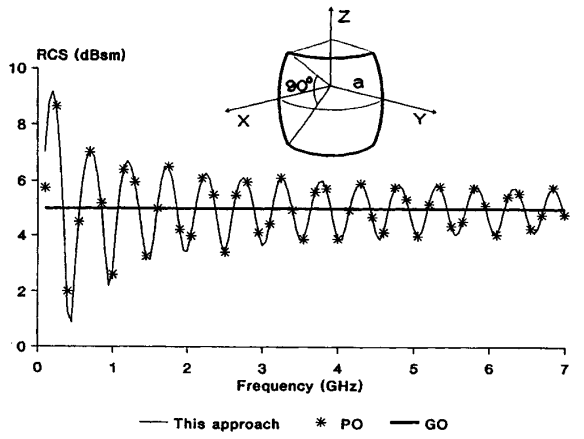

Fig. 10. RCS of a spherically curved plate at $\theta = 90°$ and $\phi = 45°$.

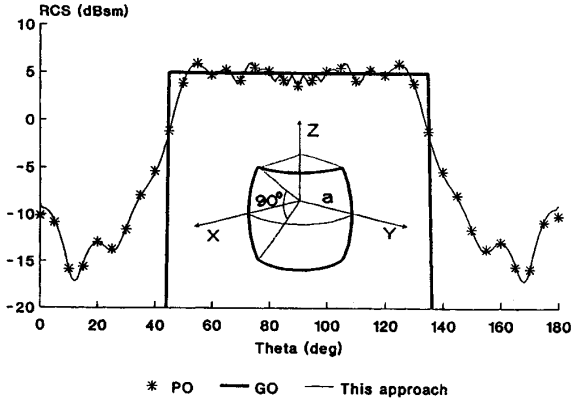

Fig. 11. RCS of a spherically curved plate along the $\phi = 45°$ cut.

are compared with GO and PO predictions. The PO values were obtained by the authors using numerical integration.

C. Conical Curved Plate

Figs. 12 and 13 show RCS results for the conical curved plate indicated in the figures. The plate has been modeled with one singly curved Bezier surface. In both cases the frequency is 1.2 GHz. The radii are $a = 1$ m and $b = 0.5$ m, the height is $h = 1$ m, and the angle $\alpha = 90°$. The plate is symmetry relative to the Y axis. The PO values were obtained by the authors using numerical integration.

D. Conesphere

This object has been modeled with four singly curved and four double curved Bezier surfaces and is sketched in Fig. 14. The sphere radius is $a = 0.974$ m, and the cone height is $h = 4.2892$ m. In Fig. 14 our result are compared with PO predictions for an angular sweep of incident waves of frequency 0.3 GHz. The PO values are obtained from [19], which uses a numerical implementation of PO.

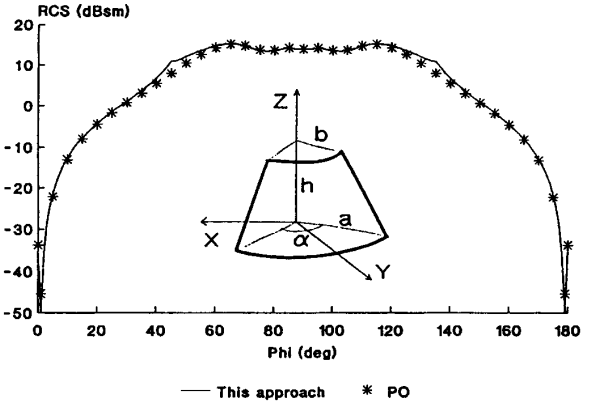

Fig. 12. RCS of a conical curved plate along the $\theta = 63.435°$ cut.

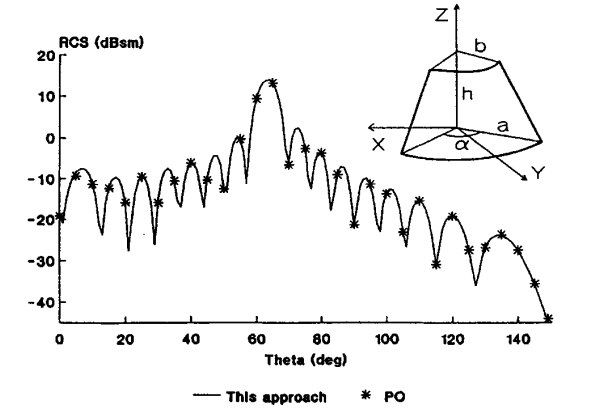

Fig. 13. RCS of a conical curved plate along the $\phi = 90°$ cut.

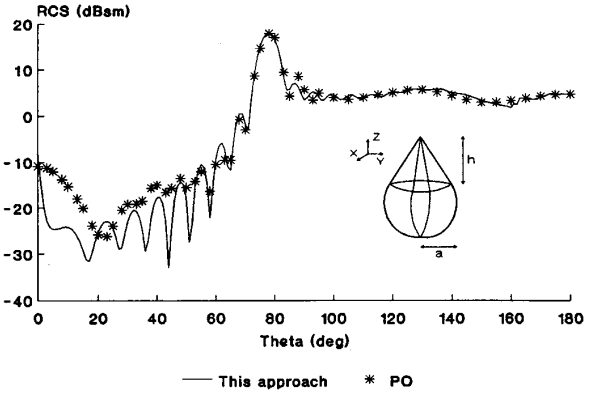

Fig. 14. RCS of a cone sphere, with Ka = 6.12 for a $\phi = cte$ cut.

VIII. Conclusion

A physical optic approach for the RCS computation of complex three-dimensional conducting bodies has been presented. This approach uses directly a description of the target in terms of NURBS surfaces that can be generated by the

most common CAGD tools. This allows us to employ for RCS predictions the same geometrical models that are used in the definition and mechanical construction of an object in an industrial environment. In curved surfaces, asymptotic techniques are used for the PO integral computation on the parametric domain. The approach is efficient because it makes use of a small number of patches to model complex bodies accurately.

The PO method fails when there are wedges on the targets surface. In this case it is necessary to take into account the Physical Theory of Diffraction (PTD) [12] correction. The authors are currently considering this and other high-frequency scattering mechanisms to analyze conducting bodies modeled by these kinds of surfaces.

NURBS and Bezier patches have been used in other works [20] to make electromagnetic analysis using the moment method.

ACKNOWLEDGMENT

The authors thank P. Brunet, R. Juan, and A. Vinacua of the Universidad Politécnica de Cataluña for their inestimable assistance in the fascinating world of modern computational geometry.

REFERENCES

[1] N. N. Youssef, "Radar cross section of complex targets," *Proc. IEEE*, vol. 77, no. 5, May 1989, pp. 722–734.
[2] R. Abad *et al.*, "Modelos matemáticos para el estudio de la RCS debida a doble reflexión, difracción en aristas y sombras por eclipse en parches poligonales planos," in *V Symposium Nacional del Comité Español de la URSI*, Vigo, September 26–28, 1990, pp. 190–194.
[3] G. Farin, *Curves and Surfaces for Computer Aided Geometric Design*. San Diego: Academic, 1988.
[4] W. Boehm, G. Farin, and J. Kahmann, "A survey of curve and surface methods in CAGD," *Computer Aided Geometric Design*, vol. 1, pp. 1–60, 1984.
[5] R. H. Bartels, J. C. Beatty, and B. A. Barsky, *An Introduction to Splines for Use in Computer Graphics and Geometric Modelling*. Los Altos, CA: Morgan Kaufmann, 1987.
[6] W. Tiller, "Rational b-splines for curve and surface representation," *IEEE Comput. Graphics Appl. 3*, pp. 61–69, Sept. 1983.
[7] J. M. Rius, M. Ferrando, and L. Jofre, "GRECO: Graphical electromagnetic computing for RCS prediction in real time," *IEEE Trans. Antennas Propagat. Mag.*, vol. 35, no. 2, pp. 7–17, Apr. 1993.
[8] W. Boehm, "Generating the Bezier points of b-spline curves and surfaces," *Computer Aided Design*, vol. 13, no. 16, pp. 365–366, 1981.
[9] E. F. Knott, "A progression of high-frequency RCS prediction techniques," *Proc. IEEE*, vol. 73, no. 2, pp. 252–264, Feb. 1985.
[10] G. T. Ruck, D. E. Barrick, W. D. Stuart, and C. K. Krichbaum, *Radar Cross Section Handbook*. New York: Plenum, 1970, Chapter 2.
[11] R. G. Kouyoumjian, "Asymptotic high-frequency methods," *Proc. IEEE*, vol. 53, pp. 864–876, Aug. 1965.
[12] E. F. Knott and T. B. A. Senior, "Comparison of the high-frequency diffraction techniques," *Proc. IEEE*, vol. 62, no. 11, pp. 1468–1474, Nov. 1974.
[13] M. Born and E. Wolf, *Principles of Optics*. London: Pergamon, 1975, pp. 752–754.
[14] L. B. Felsen and N. Marcuvitz, Radiation and Scattering of Waves. Englewood Cliffs, NJ: Prentice, 1973, pp. 370–441.
[15] L. Sirovich, *Techniques of Asymptotic Analysis*. New York: Springer, 1971, pp. 136–147.
[16] J. Pérez and M. F. Cátedra. "RCS of electrically large targets modelled with NURBS surfaces," *Electron. Lett.*, vol. 28, no. 12, pp. 1119–1121, June 1992.
[17] W. B. Gordon, "Far-field approximation to the Kirchhoff–Helmholtz representations of scattered field," *IEEE Trans. Antennas Propagat.*, vol. AP-23, pp. 864–876, July 1975.
[18] M. A. Plonus, R. Williams, and S. C. H. Wang, "Radar cross section of curved plates using geometrical and physical diffraction techniques," *IEEE Trans. Antennas Propagat.*, vol. AP-26, no. 3, pp. 488–493, May 1978.
[19] I. D. King, "RCS of perfectly conducting or coated bodies," in *Proc. Workshop JINA'90*, Nice, France, Nov. 16, 1990.
[20] L. Valle, F. Rivas, and M. F. Cátedra. "Electromagnetic scattering by arbitrary shaped bodies modeled with NURBS surfaces using the method of moments," *Nize, Journées Internationales de Nice sur les Antennes*, JINA'92, 1992, pp. 35–38.

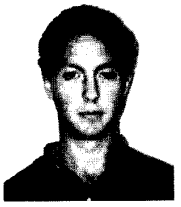

J. Pérez (S'93) was born in Santander, Spain, in 1965. He received the M.Sc. degree in physics from the University of Cantabria, Cantabria, Spain, in 1989.

Since 1989 he has been with the Electronics Department, University of Cantabria, where he is working toward his Ph.D. degree. His areas of interest include electromagnetic radiation and scattering, geometrical modeling in electromagnetics, and mobile communications.

M. F. Cátedra (S'80–M'82), for a biography please see p. 213 of the February 1993 issue of this TRANSACTIONS.